Available online at www.sciencedirect.com
SCIENCE DIRECT®
Journal of Magnetic Resonance 176 (2005) 54–63
JMR Journal of Magnetic Resonance
www.elsevier.com/locate/jmr

On-resonance low B_1 pulses for imaging of the effects of PARACEST agents

Elena Vinogradov [a,*], Shanrong Zhang [b,1], Angelo Lubag [b], James A. Balschi [d], A. Dean Sherry [b,c], Robert E. Lenkinski [a]

[a] Department of Radiology, Beth Israel Deaconess Medical Center, Harvard Medical School, 330 Brookline Avenue, Boston, MA 02215, USA
[b] The Rogers Magnetic Resonance Center, Department of Radiology, University of Texas Southwestern Medical Center, 5801 Forest Park Road, Dallas, TX 75235-9085, USA
[c] Department of Chemistry, University of Texas at Dallas, P.O. Box 830688, Richardson, TX 75083-0688, USA
[d] NMR Laboratory for Physiological Chemistry, Brigham and Woman's Hospital, Harvard Medical School, 221 Longwood Avenue, Boston, MA 02115, USA

Received 7 February 2005; revised 8 May 2005
Available online 23 June 2005

Abstract

Application of the exchange-sensitive, low-power RF pulses positioned on the bulk water resonance for imaging of the effects of PARACEST agents is proposed as an alternative to the standard CW off-resonance irradiation. Specifically, we applied a low-power WALTZ-16 RF train, with the 90° pulse unit replaced by a pulse of the fixed length (WALTZ-16*). Using this sequence, the bulk water signal was found to be sensitive to exchange lifetimes with PARACEST complex bound protons, the transverse relaxation time of bulk water, and longitudinal relaxation time of bound protons. In this report, the concept of using WALTZ-16* to "activate" a PARACEST effect is introduced and some of the salient features of this technique with respect to experimental conditions and performance levels are discussed. Computational predictions are verified and explored by comparison with experimental spectroscopic and imaging data. It is shown that WALTZ-16* can be used to detect PARACEST agents with an RF intensity as low as 200 Hz for concentrations as low as a few tens of μM for lanthanide chelates having appropriate water-exchange rates (Tm,Dy).

Keywords: PARACEST; Low B_1 WALTZ-16; Contrast; Exchange; Relaxation

1. Introduction

Image contrast in MRI reflects a variety of intrinsic properties of tissue, including the relaxation properties of water and fat, their concentrations, flow, diffusion, etc. In addition, it is possible to generate images with contrast based upon interactions between spins of various nuclei, such as chemical exchange and dipolar–dipole interactions. Magnetization transfer enhancement, introduced by Balaban and co-workers, uses long, weak, off-resonance RF pulse to saturate a broad water signal that lies beneath a sharper bulk water signal in many tissues [1]. More recently, a similar principle was applied to compounds with slowly exchanging –NH or –OH protons. Irradiation of these exchanging protons decreases the bulk water signal. This MR contrast method, chemical exchange saturation transfer (CEST) imaging [2], allows the operator to switch image contrast "on" and "off" via an RF pre-saturation pulse. As chemical exchange can be quite sensitive to the environment of a contrast agent, the CEST effect can be used to image important physiological parameters such as

* Corresponding author.
E-mail address: evinogra@bidmc.harvard.edu (E. Vinogradov).
[1] Present address: Center on Human Development and Disability, Department of Radiology, University of Washington Medical Center, Box 357115, 1959 NE Pacific Street, Seattle, WA 98195-7115, USA.

1090-7807/$ - see front matter
doi:10.1016/j.jmr.2005.05.016

pH [3–7]. A variety of endogenous and exogenous CEST agents are being explored: endogenous amide protons [4] (amide proton transfer APT) and small molecules [8] (urea); and, exogenous polymers [9] and paramagnetic lanthanide (III) complexes [5,10,11].

The exogenous paramagnetic lanthanide complexes exhibit slow lanthanide-bound water-exchange kinetics and large chemical shifts for the lanthanide-bound water molecule [11]. These highly shifted bound water protons can be selectively pre-saturated and the saturation transferred to the bulk water via chemical exchange. There are a number of the potential advantages of paramagnetic CEST (PARACEST) agents [12]. First, PARACEST agents permit the use of faster water molecule exchanging systems while remaining in the slow-to-intermediate exchange regime. Second, the selective RF pulse can be applied much further away from the bulk water, resulting in less direct saturation of the bulk water resonance. Finally, as indicated above, since the CEST effect is intrinsically sensitive to chemical exchange, it may be possible to design PARACEST agents that report important biological indices such as pH [5–7], temperature, lactate [13] or glucose [14] concentrations and oxygen or metabolite levels in vivo using a conventional MRI scanner [14].

Theory predicts that in the slow exchange limit the PARACEST effect should become larger with faster water exchange, if a sufficiently strong RF field is used for off-resonance saturation [15]. At the same time, at this faster exchange, saturation of the bound pool may require very high RF powers not available in standard human or animal imager, and may be not effective at all if exchange lifetimes are very short [15,16]. In addition, the off-resonance RF field strength may be limited in human applications by the FDA guidelines for power deposition (SAR). This limit will be a complex function of RF coil design, patient weight, and the particular imaging sequence employed. In practice, these considerations may restrict PARACEST agents to those with water-exchange lifetimes on the order of milliseconds.

Application of off-resonance irradiation is not the only way to observe effects due to chemical exchange. Many alternative ways have been exploited in solution NMR [17], a few of these have been applied to MRI. For instance, in the WEX experiment, van Zijl et al. [18,19] used a water-exchange filter to detect mobile and exchanging protons. Recently, Michaeli and coworkers [20] studied the effects of exchange on the rotating frame relaxation under the influence of adiabatic pulses and showed that the contribution of exchange to $T_{1\rho}$ can be varied by changing pulse parameters. It has also been demonstrated that fast exchanging agents can reduce the T_2 of bulk water protons by chemical exchange [17,21]. In addition, on-resonance pulses, saturating tissue with short T_2, have been used to create MT contrast enhancement [22–24]. This led us to consider the possibility of applying exchange and relaxation-sensitive pulses directly on the bulk water resonance in combination with rapid-exchange PARACEST agents. Amplitude and phase modulation of the RF train can be potentially utilized to enhance the effects of chemical exchange. Such modulated pulses provide almost endless possibilities for the design of an optimal RF train that will be sensitive to chemical exchange and substantially lower the total power deposited. Another advantage of an on-resonance strategy is that it is not necessary to know the exact position of a Ln-bound water resonance.

The problem is to design such an RF train. The simplest form of pulse would be application of a long, low-power 360° pulse on bulk water resonance (similar to the binomial pulses used for MT contrast). At the termination of the pulse, non-exchanging water spins will return to the Z axis while any exchanging protons might "leak away" during the long RF pulse and, hence, not experience the full 360° rotation. The result would be a decrease in Z magnetization, much like that experienced in a conventional CEST experiment. Such pulses, however, may be impractical for the in vivo applications since they are quite sensitive to RF and B_0 inhomogeneities. To overcome inhomogeneity issues, composite pulses [25] can be used. Bearing this in mind, we have investigated the use of a low-power WALTZ-16 [26,27] pulse train to achieve visualization of the effects due to the presence of the PARACEST contrast agents.

In this report, the concept of using WALTZ-16 to "activate" a PARACEST effect is introduced, and some of the salient features of this technique with respect to experimental conditions and performance levels are discussed. Computational predictions are verified and explored by comparison with experimental spectroscopic and imaging data.

2. Theoretical background

Chemical exchange transfers magnetization from pool B (bound water) to pool A (bulk water) and vice versa. The following Bloch–McConnell equations describe the dynamics of the magnetization of both pools [15]:

$$\frac{dM_x^a}{dt} = -\delta_a M_y^a - (R_{2a} + k_a) M_x^a + k_b M_x^b + \omega_1(t) \sin\phi(t) M_z^a, \tag{1}$$

$$\frac{dM_y^a}{dt} = \delta_a M_x^a - (R_{2a} + k_a) M_y^a + k_b M_y^b - \omega_1(t) \cos\phi(t) M_z^a, \tag{2}$$

$$\frac{dM_z^a}{dt} = R_{1a} M_0^a - (R_{1a} + k_a) M_z^a + k_b M_z^b - \omega_1(t) \sin\phi(t) M_x^a + \omega_1(t) \cos\phi(t) M_y^a, \tag{3}$$

$$\frac{dM_x^b}{dt} = -\delta_b M_y^a - (R_{2a} + k_b)M_x^b + k_a M_x^a + \omega_1(t)\sin\phi(t)M_z^b, \tag{4}$$

$$\frac{dM_y^b}{dt} = \delta_b M_x^b - (R_{2b} + k_b)M_y^b + k_a M_y^a - \omega_1(t)\cos\phi(t)M_z^b, \tag{5}$$

$$\frac{dM_z^b}{dt} = R_{1b}M_0^b - (R_{1b} + k_b)M_z^b + k_a M_z^a - \omega_1(t)\sin\phi(t)M_x^b + \omega_1(t)\cos\phi(t)M_y^b, \tag{6}$$

where

$$R_{1a,b} = 1/T_{1a,b}, \tag{7}$$

$$R_{2a,b} = 1/T_{2a,b}, \tag{8}$$

$$\delta_{a,b} = \omega - \omega_{a,b}. \tag{9}$$

In these equations ω_a is the Larmor frequency of pool A, T_{1a} is the spin–lattice relaxation time of pool A, T_{2a} is the transverse relaxation time of pool A, and k_a is the transition rate of A nuclei leaving pool A and is equal to $1/\tau_a$, where τ_a is the life time of a proton in A. Similar definitions apply to B nuclei. The value of k_a is determined by the detailed-balance relationship

$$k_a = \left(\frac{M_0^b}{M_0^a}\right)k_b = \left(\frac{M_0^b}{M_0^a}\right)\frac{1}{\tau_b}. \tag{10}$$

The value of k_a is enhanced by increasing the concentration of a PARACEST agent and by decreasing lifetimes of the protons in the bound pool (B). The thermal equilibrium Z magnetizations, M_0^a and M_0^b, are directly proportional to the number of protons in pools A and B, respectively; these quantities are determined by the composition of the system.

In addition, in Eq. (9), ω is the frequency of the RF irradiation, $\omega_1(t)$ is its amplitude, and $\phi(t)$ is its phase. Eqs. (1)–(6) assume the same rotating frame for both pools, and the time dependence of the RF irradiation due to high off-resonance values of the B pool was ignored. In principle, both the phase and amplitude of the RF irradiation can be time dependent. In the WALTZ-16 train the amplitude remains constant, while the phase is time dependent. Due to this time dependence, there is no analytical solution of these equations. Furthermore, for many of the PARACEST compounds, the system is in an intermediate-to-slow exchange regime with $k_{ex} = k_a + k_b$ of the same order of magnitude or higher than Δ. Analytical theoretical approaches beyond fast-exchange regime are not widely reported [28–30]. Hence, numerical simulations need to be applied in order to study magnetization dynamics.

There are a number of intrinsic system parameters that can potentially influence the sequence performance: T_{1a}, T_{1b}, T_{2a}, T_{2b}, and τ_a, the chemical shift difference between protons in A and B ($\Delta = \omega_a - \omega_b$), and the concentration of the agent. In addition, there are experimental imperfections, such as RF (B_1) and B_0 homogeneities. To elucidate the influence of these parameters, simulations and experiments were performed, and those results will be presented in the following sections.

3. Materials and methods

3.1. Computational methods

A set of MATLAB computer programs was written to calculate the magnetization dynamics under the influence of a low-power WALTZ-16 pulse train as a function of RF amplitude, off-resonance frequency of bulk water, and relaxation and exchange parameters of the system. The simulations employ stepwise integration of the time-dependent Bloch–McConnell equations (Eqs. (1)–(6)).

3.2. Experimental

Experiments were performed on either a Varian Unity INOVA 400 MHz (9.4T) vertical wide-bore (89 mm) spectrometer or a Varian Unity INOVA 200 MHz (4.7T) horizontal wide-bore imaging scanner. The spectroscopy experiments were performed on the INOVA 400 machine using a 5 mm liquid NMR double channel probe. The imaging experiments were performed at both 200 and 400 MHz field strengths. In the former case, a surface coil with the diameter of 2 cm was employed and in the latter a 30 mm imaging probe with an imaging gradient coil.

3.3. WALTZ-16* pulse train

In our experiments, we have employed a WALTZ-16 pulse train consisting of [26,27]:

$$(3t_p)_{180}(4t_p)_0(2t_p)_{180}(3t_p)_0(t_p)_{180}(2t_p)_0(4t_p)_{180}(2t_p)_0(3t_p)_{180}$$
$$(3t_p)_0(4t_p)_{180}(2t_p)_0(3t_p)_{180}(t_p)_0(2t_p)_{180}(4t_p)_0(2t_p)_{180}(3t_p)_0$$
$$(3t_p)_0(4t_p)_{180}(2t_p)_0(3t_p)_{180}(t_p)_0(2t_p)_{180}(4t_p)_0(2t_p)_{180}(3t_p)_0$$
$$(3t_p)_{180}(4t_p)_0(2t_p)_{180}(3t_p)_0(t_p)_{180}(2t_p)_0(4t_p)_{180}(2t_p)_0(3t_p)_{180},$$

where subscripts indicate the phase of the pulse and t_p is the pulse length. In the WALTZ-16 experiment, the t_p is equal to the length of 90° pulse. In our experiments, t_p was fixed at 2.5 ms, which did not necessarily correspond to 90° pulse. Those later experiments are referred to as WALTZ-16* to distinguish them from the original WALTZ-16*. The total length of the pulse train was 220 ms. Based on simulations (see Section 4), experiments were then performed in the B_1 range of 100–300 Hz.

3.4. Spectroscopy experiments

A standard 90° pulse sequence was modified by adding a WALTZ-16* train before the 90° pulse. Integrated signal intensities were measured with and without the application of the pulse train. The intensity of the signal without WALTZ-16* corresponds to the total initial magnetization of bulk water, (M_0^a), while the signal intensity after including the WALTZ-16* pulse train corresponds to the total Z magnetization of water at the end of the RF train, (M_z^a). All data are then reported as a relative magnetization, M_z^a/M_0^a. A decrease in M_z^a/M_0^a corresponds to a lower intensity of bulk water and, in an imaging experiment, to reduction in image intensity. Six samples were prepared containing either 1 mM, 600, 250, 125, and 12.5 μM TmDOTAM (see Scheme 1 for the chemical structure) or deionized water with D_2O added for shimming purposes. Pool B to A ratios in these samples are 18.2×10^{-6}, 10.9×10^{-6}, 4.5×10^{-6}, 2.3×10^{-6}, 0.23×10^{-6}, and 0, respectively. In the spectroscopy experiments the field was intentionally de-shimmed to better mimic the in vivo situation.

To study the MT effects and the behavior in a semi-solid system, two phantoms containing (1) 0.5% agarose gel and (2) 0.5% agarose gel with 50 μM TmDOTAM (pool B to A ratio 0.9×10^{-6}) were prepared.

3.5. Imaging

A standard spin-echo sequence was employed with a WALTZ-16* pulse applied before the imaging pulses. Two images were acquired: (1) with a WALTZ-16* train applied far off-water resonance (effectively WALTZ irradiation off) and (2) WALTZ-16* applied on the bulk water resonance (WALTZ irradiation on). A relative difference image was then reconstructed via a pixel-by-pixel calculation according to the formula

$$\frac{(I_{\text{off}}-I_{\text{on}})}{I_{\text{off}}}, \tag{11}$$

where I_{off} and I_{on} correspond to the signal intensity with the WALTZ-16* pulse off and on, respectively.

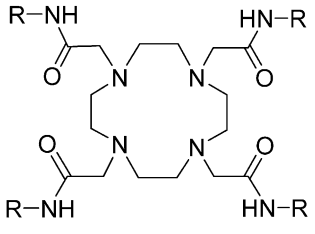

R = H **DOTAM**

CH2COOEt **DOTA-4AmCE**

Scheme 1.

In the experiments performed on the 400 MHz spectrometer, a phantom containing four tubes with different concentrations of TmDOTAM was imaged: (1) 1 mM, (2) 125 μM, (3) 12.5 μM, and (4) water (pool B to A ratios of (1) 18.2×10^{-6}, (2) 2.3×10^{-6}, (3) 0.23×10^{-6}, and (4) 0). The imaging parameters were FOV = 25×25 mm^2, TR = 30 s, TE = 30 ms, matrix size varied between 32×32 to 128×128 in different experiments with a slice thickness of 2 mm.

In experiments performed at 200 MHz a phantom containing four tubes with different concentrations of DyDOTAM was imaged: (1) 2 mM, (2) 1 mM (3) 125 μM, and (4) tube with water (pool B to A ratios of (1) 36.4×10^{-6}, (2) 18.2×10^{-6}, (3) 2.3×10^{-6}, and (4) 0). The imaging parameters were FOV 20×20 mm^2, TR = 1 s, TE = 15 ms, matrix size 256×256, slice thickness 2 mm, and in-plane resolution of 78×78 μm^2. In addition, a phantom containing different concentrations of TmDOTA-4AmCE was imaged: (1) 41 μM, (2) 15 μM, (3) 7.3 μM, and (4) water (pool B to A ratios of (1) 0.75×10^{-6}, (2) 0.27×10^{-6}, (3) 0.13×10^{-6}, and (4) 0).

4. Results and discussion

4.1. Computational results

4.1.1. RF performance

First, the influence of the low-power WALTZ-16* (less than 1 kHz RF intensity) on water in the absence of exchange was estimated. In principle, the train corresponds to a complete 360° rotation and, hence, should have no influence on total Z magnetization. The intensity can, however, be influenced by T_{1a} and T_{2a} of water and the amplitude and offset of the RF irradiation. Of particular importance in the experiment is the robustness with respect to B_1 field inhomogeneity (RF irradiation amplitude dispersion) and B_0 field inhomogeneity (RF irradiation offset dispersion). The high-power WALTZ-16 is well compensated for both power and field inhomogeneities; however, at low-power levels its performance may deteriorate [31]. In addition, relaxation effects will also influence the performance and the amount of the M_z/M_0 at the end of the train even in a system without exchange. To determine the robustness of the low-intensity WALTZ-16* train, the dependence of the Z magnetization on the RF intensity and offset was simulated in pure water. The relative magnetization size, M_z/M_0, as a function of RF intensity ($\omega_1/2\pi$) and offset (δ_a) is shown in Fig. 1. In these simulations, as well as in actual experiments, the pulse length was constant, while RF intensity and offset varied. T_1 was assumed to be equal to 5 s and T_2 to be 2.5 s. It is desirable to have M_z/M_0 unchanged and equal to 100% over as wide a range of RF intensities and offsets as possible. The sim-

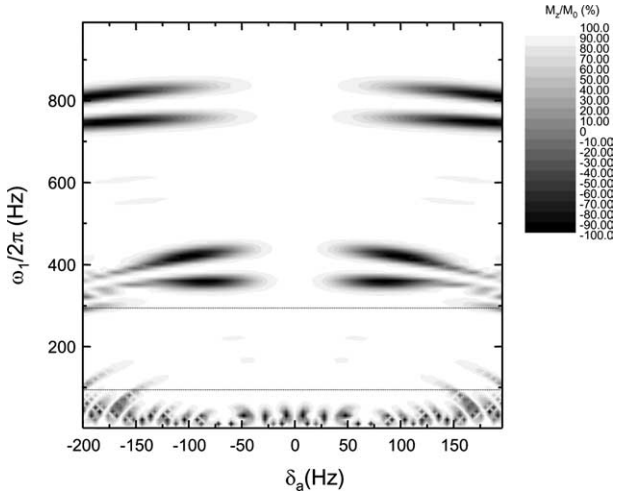

Fig. 1. Simulations of relative magnetization size, M_z/M_0, where M_z is the Z-magnetization after the application of the WALTZ-16* and M_0 is the initial magnetization, as a function of RF intensity ($\omega_1/2\pi$) and offset (δ_a) in the system without exchange. Dotted lines designate the preferable region for experiments, where M_z/M_0 remains constant over the wide range of RF intensity and offsets. In this region, the influence of RF and B_0 inhomogeneity is minimal.

ulation (Fig. 1) shows that WALTZ-16* RF power and offset influence M_z/M_0. In experiments, the RF intensity should be chosen to minimize the variations in M_z/M_0. Low-power WALTZ works well only in certain B_1 intensity regions. It is particularly poor between ~300 and 425 Hz, where the magnetization is inverted (M_z/M_0 negative). The desirable intensity range is between 100 and 300 Hz (dashed horizontal lines), where magnetization is around 93% throughout most of the region. In this amplitude range, the pulse performance is very stable over a range of frequency offsets. The gap between "bad" areas is 400 Hz, precisely equal to $1/t_p$. The position of "bad" and "good" areas changes for different t_p values with a gap equal to $1/t_p$. Further theoretical treatment of this effect is beyond the scope of the present paper.

Using a T_1 of 5 s, a T_2 of 2.5 s, and a B_1 field of 200 Hz, the pure water magnetization decreases to 93% (Fig. 1). This decrease results from the T_2 relaxation during the WALTZ-16*. Contrast due to the PARACEST exchange will be achieved if the presence of the exchanging protons further decreases M_z^a/M_0^a of the bulk water. Hence, in the ensuing sections the results will be compared with the M_z/M_0 of the pure water.

4.1.2. System parameters influence

Simulations of the magnetization ratio, M_z^a/M_0^a, as a function of free water-exchange lifetimes τ_a and chemical shift difference, Δ, were performed (Fig. 2). A 9.4T B_0 field and 100 μM concentration (pool B to A ratio of 1.8×10^{-6}) of the PARACEST agent were assumed, with $T_{1a}=5$ s, $T_{2a}=2$ s, and $T_{1b}=T_{2b}=0.2$ s. The

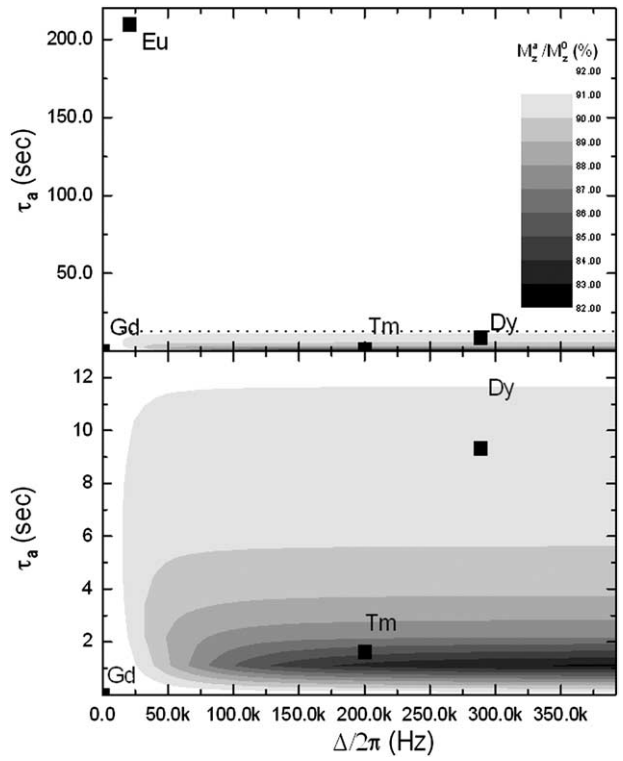

Fig. 2. Simulations of the decrease of the free water relative magnetization, M_z^a/M_z^0, as a function of the free water-exchange lifetime (τ_a) and chemical shift difference ($\Delta/2\pi$). The lower graph shows an expanded area confined by the dotted line in the upper graph. Values of τ_a and $\Delta/2\pi$ typical for Eu, Tm, Dy, and Gd complexes are indicated on the graph, assuming exchange lifetimes and chemical shifts of Ln–DOTA-4AmCE compounds (Table 1) and 400 MHz B_0 field. Values of M_z^a/M_z^0 vary from 82% (black) to 92% (white) in the increments of 1%. Simulation parameters are detailed in the text.

simulated contrast, M_z^a/M_0^a, should be compared with pure water magnetization ratio ($M_z/M_0=93\%$). Experimentally measured values of τ_a and Δ for typical Eu-, Tm-, and Dy-based PARACEST agents are indicated on the graph. The Ln–DOTA-4AmCE complex exchange lifetimes and chemical shifts change with Ln size [11] (Table 1). For typical Gd-based relaxation agents, a zero chemical shift difference and nanosecond exchange lifetime was assumed. To achieve a maximal effect, free water-exchange lifetimes of the order of 0.5–1 s are desirable, with the largest possible chemical shift of the bound water. The Tm and Dy compounds provide the largest effect. Both of these agents have short exchange

Table 1
Exchange lifetimes and chemical shifts for some of the Ln–DOTA-4AmCE chelates and typical value for the Gd^{3+} complexes

Lanthanide ion	τ_b (μs)	Δ (ppm)
Eu^{3+} [a]	382	50
Dy^{3+} [a]	17	−720
Tm^{3+} [a]	3	500
Gd^{3+}	0.001	0

[a] Reproduced from [33].

lifetimes and short T_{1b} values prohibiting efficient suppression at low RF powers and providing a very small effect with off-resonance CW saturation. The exchange lifetime, τ_a, can be decreased by increasing agent concentration (see Eq. (2)), but a chemical shift difference cannot be changed for a specific Ln ion. Hence, complexes with smaller Δ, like Eu, are not as favorable for this type of experiment. These results can be understood intuitively by viewing the process as a leak or drain of magnetization from the on-resonance pool A due to exchange. When the pulse is applied, part of the magnetization "leaks away" via the exchange and, hence, does not experience a full 360° rotation. Consequently M_z^a is decreased. The bigger chemical shift difference, the less effect the pulses will have on the "escaping" magnetization.

In the presence of RF irradiation, the magnetization behavior is governed by longitudinal and transverse relaxation times in the interaction frame, $T_{1\rho}$ and $T_{2\rho}$, governing relaxation parallel and perpendicular to the RF effective field, respectively. The exact analytical solution for $T_{1\rho}$ in the presence of composite pulses currently is not available. In addition, WALTZ-16* is not cyclic for all RF off-resonance and intensity values [31]. Under the conditions when the WALTZ-16* irradiation is cyclic (e.g., exactly on-resonance or when $t_p\omega_1 = \pi/2$), the behavior of the Z magnetization at the end of the WALTZ-16* train will be governed by $T_{1\rho}$. Based on the theoretical treatments of exchange in the presence of CW [28,29,32] and adiabatic pulses [20], it can be assumed that the $T_{1\rho}$ will contain contributions from T_2, exchange lifetimes, and T_1. Hence, the effective decrease will be determined not only by exchange parameters but also by the T_{2a} and T_{1a} of bulk water. To study this effect, the magnetization ratio M_z^a/M_0^a was simulated as a function of τ_a and T_{2a}, Fig. 3. This simulation assumed a chemical shift difference of 500 ppm (typical of Tm complexes), a 9.4T B_0, a B_1 intensity of 200 Hz, and an agent concentration of 100 μM (pool B to A ratio of 1.8×10^{-6}). The simulated results indicate that T_{2a} will have a strong influence on the total decrease in M_z^a/M_0^a. It is evident from the data that for a T_2 on the order of 0.4 s or higher, the biggest decrease is observed for τ_a of 0.4–1 s. In this region the total effect size will be determined by both T_{2a} and τ_a. Hence, strong relaxation agents, like Gd complexes will provide a big effect in this type of experiment.

Based on these results, it follows that for quantitative measurements in tissues two experiments need to be performed: one before contrast injection to quantify signal decrease due to intrinsic T_{2a}, and one after the injection. The relative signal difference between the two experiments will give a quantitative measure of the exchange-mediated effects.

It also follows that in a semi-solid tissue with short T_{2a}, saturation will also be created, thus leading to

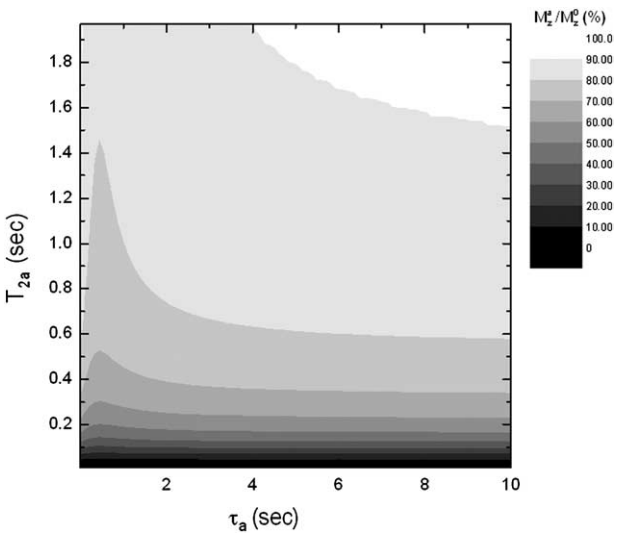

Fig. 3. Simulations showing the decrease of the free water relative magnetization, M_z^a/M_z^0, as a function of the free water-exchange lifetime (τ_a) and transverse relaxation time (T_{2a}). Values of M_z^a/M_z^0 vary from 0% (black) to 100% (white) in the increments of 10%. A chemical shift difference of 500 ppm (typical of Tm complexes) and 400 MHz B_0 field was assumed. Other simulation parameters are detailed in the text.

MT effects. However, if two experiments are performed, as described before, the MT effects will be canceled.

The influence of the T_{1a} was simulated, at 100 μM (pool B to A ratio of 1.8×10^{-6}), a B_0 of 9.4T, and $T_{1b} = T_{2b} = 0.2$ s. Using T_{2a} values between 0.01 and 2 s, the T_{1a} was varied between T_{2a} and 10 s. Both relaxation times have an influence when they are the same order of magnitude as the RF train length, i.e., less than 1 s. Again, T_{2a} has a much stronger influence on the determination of the total effect size than T_{1a}. Overall, for T_{1a} values of 1 s and longer or for $T_{1a} \gg T_{2a}$, the decrease in the magnetization has a very weak dependence on T_{1a}.

The influence of T_{1b} and T_{2b} was also simulated. For T_{1b} of the order of 100 μs and higher, the effect is found to be negligible, and the total effect size is governed by the relaxation and exchange parameters of the free water. However, very short T_{1b} values, of the order of few tens of microseconds and lower, do influence the effect size. For 100 μM of a contrast agent (pool B to A ratio of 1.8×10^{-6}) with an exchange lifetime of 3 μs, varying T_{1b} between 10 and 100 μs results in M_z^a/M_0^a change of 5%. Very short T_{1b} results in "memory loss" of the magnetization residing in the bound state. The bound lifetime is very short, however, it is long enough for partial or full return of the magnetization to the initial state. Hence, magnetization will go astray from the WALTZ dictated trajectory, and the observed M_z^a/M_0^a will decrease. Short T_{1b} enhances exchange-mediated dephasing mechanism. This suggests that even very effective relaxing ions, such as Dy^{3+} and Tb^{3+}, could be used in this type of experiment.

To summarize, the total effect size will be governed by T_{2a}, τ_a, and T_{1b}.

5. Experimental results

5.1. Spectroscopy

Spectroscopy measurements were performed to validate the simulations and to estimate the signal decrease in real systems. Since the largest effect (decrease in M_z^a/M_0^a) was predicted for Tm compounds, solutions containing variable concentrations of TmDOTAM ([TmDOTAM]) as a prototype agent were investigated. The offset behavior was verified by shifting the frequency of the WALTZ-16* train from that of bulk water and measuring M_z^a/M_0^a (Fig. 4). The B_1 field was fixed and approximately equal to 200 Hz. To estimate the dispersion of the results over the off-resonance range, the mean and standard deviation of M_z^a/M_0^a were calculated. The values for the [TmDOTAM] are as follows: $90.6 \pm 0.8\%$ for pure water (0 μM), $86 \pm 0.9\%$ for 12 μM, $75 \pm 2\%$ for 125 μM, $64 \pm 1\%$ for 250 μM, $40 \pm 2\%$ for 600 μM, and $27 \pm 3\%$ for 1000 μM. From these values and from the figure it is evident that the M_z^a/M_0^a varies less than 10% for offsets of ±100 Hz. This variation increases with effect size, with larger deviations for samples containing higher [TmDOTAM]. In an imaging experiment, B_0 inhomogeneities are expected to be higher than in the high-resolution experiments so one would anticipate a larger standard deviation in the signal decrease for samples measured in an imaging versus a spectroscopy measurement.

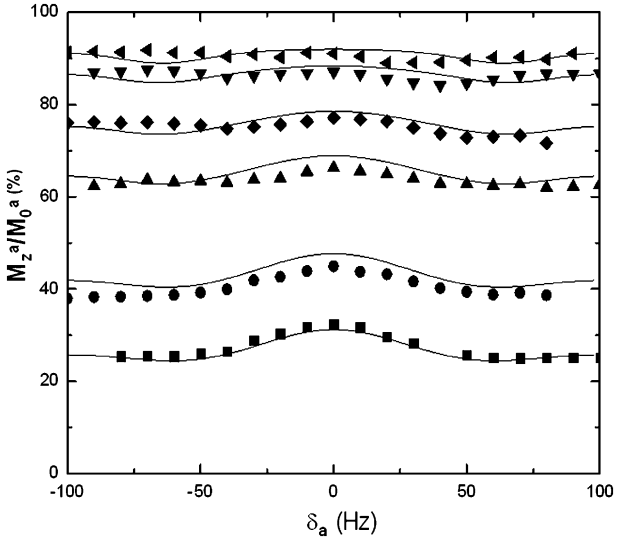

Fig. 4. Experimental measures of M_z^a/M_0^a at 400 MHz B_0 field after application of a WALTZ-16* pulse train using a fixed RF intensity of 200 Hz and variable RF offsets (δ_a). Each symbol represents a different [TmDOTAM]: ■, 1 mM; ●, 600 μM; ▲, 250 μM; ♦, 125 μM; ▼, 12.5 μM; and ◀, 0 (water only). The solid lines correspond to the simulations that best matched the experimental results visually. The simulation parameters are given in the text.

Simulated results (solid lines) are also shown in Fig. 4. The simulation parameters were derived as follows: T_{1a} values were measured experimentally and are 4.2, 4.0, 3.8, 3.9, 2.4, and 2.2 s for water, 12.5, 125, 250, 600 μM, and 1 mM, respectively. The displayed T_{1a} shortening can be attributed to the exchange effects [17,21]. T_{2a} values, also influenced by exchange, were measured using CPMG in water and 12.5 μM solution and are equal to 2.02 and 1.48 s, respectively. Relaxation times measured in the water sample were longer than expected from exchange contribution alone, probably because of the addition of D_2O. T_{1a} and T_{2a} values used in the simulations were taken as equal to the values measured in 12.5 μM solution. The assumption was that at this low concentration the exchange-mediated changes in the relaxation times will be minor to negligible. In the simulations, an exchange lifetime for the bound water of TmDOTAM was assumed equal to $\tau_b = 2.6$ μs, a value close to the experimentally measured 3 μs for an analogous compound, TmDOTA-4AmCE [33]. T_{1b} and τ_b were the parameters varied to achieve the simulation that best matched the experimental results visually. Note that since the total effect size is governed by T_{2a}, T_{1b}, and τ_a there might be another set of parameters producing similar effect sizes. The purpose of the simulation was to provide a qualitative description of the experimental results.

The RF inhomogeneity dependence was verified by varying the RF intensity level of the WALTZ-16* train while fixing the frequency of the RF irradiation to that of bulk water. These results are shown in Fig. 5, together with the best visually matched simulations. The simulation parameters were the same as described above except that in some cases an offset of 10–20 Hz was assumed. These offsets may come from B_0 fluctuations in the spectrometer due to a nearby subway. In the 100–300 Hz range the effect size was 90 ± 1, 86 ± 2, 77 ± 1, 65 ± 1, 44.6 ± 0.6, and $30 \pm 1\%$ for water, 12.5, 125, 250, 600, and 1000 μM, respectively. These values are in agreement with the average values measured before. The simulation shows a few dips between 300 and 500 Hz, consistent with the "bad areas" predicted in Fig. 2. In the experiments, those dips are smoothed out, probably due to the above-mentioned field inhomogeneities and field fluctuations.

Overall, the effective decrease in the free water signal due to the presence of TmDOTAM was 4% for 12.5 μM, 14% for 125 μM, 26% for 250 μM, 53% for 600 μM, and 61% for 1 mM agent.

5.1.1. Imaging

Typical images of the phantoms containing various [TmDOTAM] measured at 400 MHz are presented in Fig. 6. These phantoms are tubes (maximum diameter

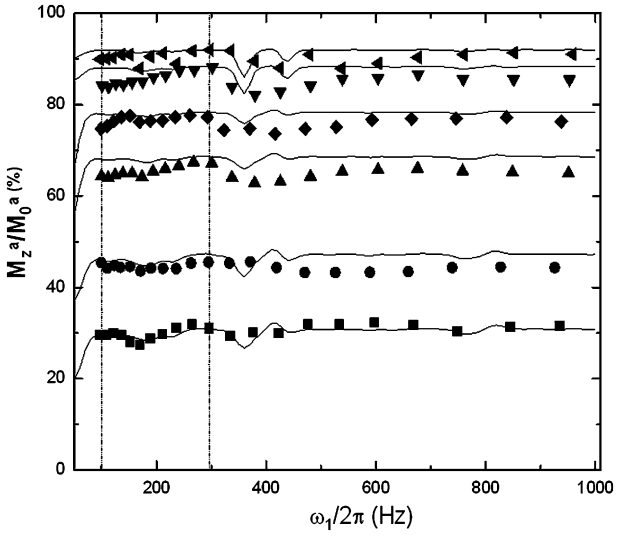

Fig. 5. Experimental measures of M_z^a/M_0^a at 400 MHz B_0 field after application of a WALTZ-16* pulse train at zero offset and different RF intensity levels ($\omega_1/2\pi$). Each symbol represents a different [TmDOTAM]: ■, 1 mM; ●, 600 μM; ▲, 250 μM; ♦, 125 μM; ▼, 12.5 μM; and ◀, 0 (water only). The solid lines correspond to the simulations that best matched the experimental results visually. The simulation parameters are given in the text. The vertical dotted lines mark an optimal region of $\omega_1/2\pi$ for the experiment.

8 mm) filled with the solutions of TmDOTAM. Fig. 6A shows a spin-echo image of the phantom with a WALTZ-16* pulse applied far off-resonance, and Fig. 6B shows the same slice but with WALTZ-16* on bulk water. Contrast is clearly seen in all samples except the sample containing 12.5 μM TmDOTAM. To quantify the effect and compare it to the spectroscopic results, the relative difference image was calculated according to Eq. (11) and is shown in Fig. 6C. In this experiment the relative differences (Eq. (11)) were equal to $11.0 \pm 0.5\%$ ($M_z^a/M_z^0 = 89\%$) for water, $12.5 \pm 0.9\%$ ($M_z^a/M_z^0 = 87.5\%$) for 12.5 μM, $25.2 \pm 0.6\%$ ($M_z^a/M_z^0 = 74.8\%$) for 125 μM and $62 \pm 1\%$ ($M_z^a/M_z^0 = 38\%$) for 1 mM. The ratios measured by spectroscopy experiments were, within error, identical to those measured by imaging at the same B_0. As anticipated, the error in the relative magnetization measured by imaging is somewhat larger than that measured by spectroscopy due to poorer B_0 and B_1 homogeneities combined with lower signal-to-noise ratio in the imaging probe versus high-resolution probe. For imaging, the enhancement ratio of 12.5 μM TmDOTAM was within error identical to that of water.

Images were also acquired for a phantom containing different [DyDOTAM] at 200 MHz field using a surface coil. These results are presented in Fig. 7. The relative differences in this case are equal to $24 \pm 6\%$ ($M_z^a/M_z^0 = 76\%$) for water, $36 \pm 5\%$ ($M_z^a/M_z^0 = 64\%$) for 125 μM, $64 \pm 4\%$ ($M_z^a/M_z^0 = 36\%$) for 1 mM and $82 \pm 3\%$ ($M_z^a/M_z^0 = 18\%$) for 2 mM DyDOTAM. The effective decrease in the free water signal due to the pres-

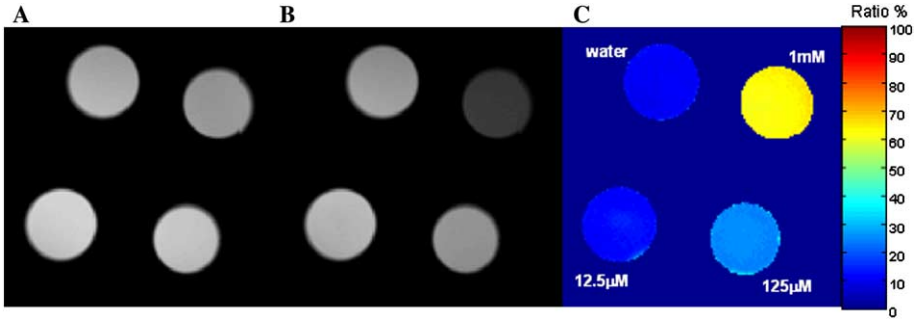

Fig. 6. Spin-echo images collected at 400 MHz of phantoms containing water and different [TmDOTAM]: 12.5 μM, 125 μM, and 1 mM. Images with WALTZ-16* placed very far off-resonance (effectively switched off) (A), on-resonance (B), and a relative difference image (C). The imaging parameters were TR/TE = 9 s/30 ms, FOV = 25×25 mm^2, matrix size 128×128, and NEX = 16.

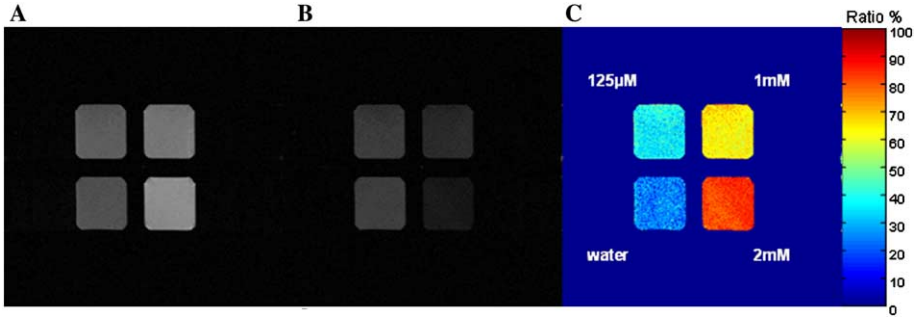

Fig. 7. Spin-echo images at 200 MHz of phantoms containing water and different [DyDOTAM]: 125 μM, 1 mM, and 2 mM. Images with WALTZ-16* placed very far off-resonance (effectively switched off) (A), on-resonance (B) and a relative difference image (C). The imaging parameters were TR/TE = 1 s/15 ms, FOV = 20×20 mm^2, matrix size 256×256, and NEX = 1.

ence of DyDOTAM is about 12% for 125 μM, 40% for 1 mM, and 58% for 2 mM agent.

To verify the performance at lower concentrations, phantoms containing different [TmDOTA-4AmC] (a different ligand only, Scheme 1) and water were also imaged at 200 MHz. At the RF intensity of 180 Hz, the relative differences were approximately 19% ($M_z^a/M_z^0 = 81\%$), 25% ($M_z^a/M_z^0 = 75\%$), 28% ($M_z^a/M_z^0 = 72\%$), and 32% ($M_z^a/M_z^0 = 68\%$) for water, 7.3, 15, and 41 μM TmDOTA-4AmC, respectively. The standard deviation of the magnetization ratios between pixels was about 5%.

5.2. Effect size versus concentration

Fig. 8 summarizes the experimental results and shows the relative magnetization decrease achieved for different [TmDOTAM] in spectroscopic and imaging experiments. The agreement between spectroscopic and imaging experiments is good, with imaging M_z^a/M_z^0 being somewhat lower than spectroscopy. In the spectroscopy experiments, concentrations as low as 12 μM can be distinguished. In imaging experiments, the errors were somewhat higher yet, on average, the image intensity of a sample containing 12.5 μM TmDOTAM can be distinguished from that of pure water. In practice, however, concentrations of 30–100 μM will be needed to produce an obvious contrast effect.

It is evident that the total effect size is determined by τ_a, T_{2a}, and T_{1b} at the specific [PARACEST] (Fig. 8). Solid line shows a simulated dependence of the decrease of M_z^a/M_0^a of TmDOTAM compound as a function of concentration. T_{2a} plays a major role in the determining the effect size. It is tempting to speculate that the results suggest that the total effect originates in changes in transverse relaxation rates due to exchange and the chemical shift effect of the paramagnetic complex. These changes should be possible to detect and quantify with T_2-sensitive experiments.

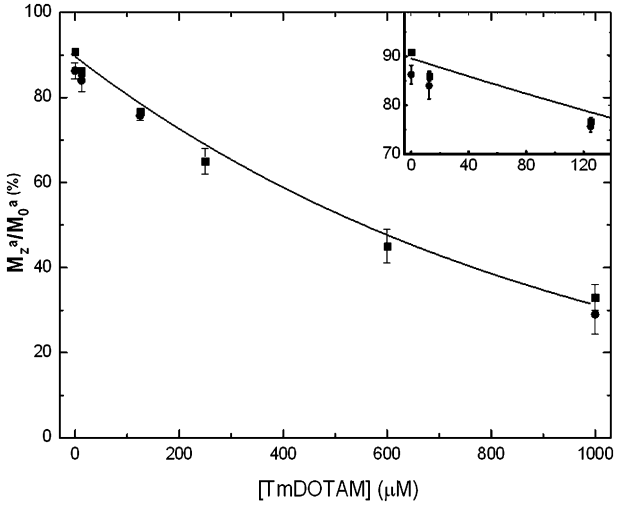

Fig. 8. Summary of experimental measures of M_z^a/M_0^a for different [TmDOTAM] after an application of a 200 Hz WALTZ-16* pulse train on resonance. Squares and circles correspond to the spectroscopy and imaging results, respectively. The concentration region, 10–200 μM, is shown expanded in upper right corner. Solid line shows a simulated dependence of the decrease of M_z^a/M_0^a as a function of [TmDOTAM].

To study the MT effects and the behavior in the semi-solid system, experiments with agarose phantoms were performed. First, the effect sizes were measured spectroscopically. As expected, WALTZ-16* resulted in decrease of the signal in agarose, with M_z^a/M_0^a after the pulse application of 33%. Addition of Tm resulted in a further decrease of the relative magnetization to about 5% (effective decrease of 27%). These spectroscopy results were confirmed qualitatively by imaging, with M_z^a/M_0^a of $20 \pm 7\%$ and $9 \pm 5\%$ for agarose and agarose + Tm phantoms, respectively. The big error in imaging values stems from the irregular shape of the phantom and large susceptibilty artifacts. Overall, these results support the view that the WALTZ-16* can be used in a semi-solid system to visualize effects due to the presence of the PARACEST agents with suitable exchange and relaxation parameters (Tm,Dy).

For comparison purposes, Z spectra measured with 5 s CW irradiation were recorded for 1 mM samples of TmDOTAM and DyDOTAM. In the Tm sample 5 kHz RF resulted in no detectable effect. In Dy 2 kHz irradiation resulted in almost 7% reduction. A comment should be made about compounds with slower exchange lifetimes and longer T_{1b} and T_{2b}, like Eu complexes. In these compounds off-resonance CW irradiation is efficient (e.g., application of CW irradiation of 1 kHz intensity on bound water peak for 1 s in 2mM EuDOTAM compound results in a 4% reduction of the signal). At the same time WALTZ-16* is not that efficient. Hence, WALTZ-16* can potentially serve as a complementary experiment in compounds with short exchange and relaxation times.

Finally, a comment should be made about the model system assumed in the simulations. We have assumed a two-pool model, while in reality there are at least three pools: bulk water, bound water, and amide protons. This third pool of the exchanging protons will definitely influence the exchange and relaxation parameters of the bulk water. However, the overall agreement between experimental results and the two-pool simulation was satisfactory and in this stage the third pool was not included.

6. Conclusions

A low-power WALTZ-16* train was employed for contrast generation of PARACEST agents. Based on both simulations and experiments, this pulse can be used

to visualize effects of PARACEST agents in concentrations as low as 30–100 μM with an RF field as low as 200 Hz. We hope that with further modifications and improvements it should be possible to detect 20–50 μM range in vivo. WALTZ-16* is sensitive to exchange lifetimes and transverse relaxation times of bulk water. The sensitivity to T_{2a} and MT effects might be a major drawback of this sequence, requiring acquisition of a reference image for quantitative studies. However, this is only one example of possible contrast generation by phase- and amplitude-modulated RF pulses. This path can potentially lead to more sensitive and less power demanding RF trains. Work is in progress to verify if this approach can be used in vivo.

References

[1] S.D. Wolff, R.S. Balaban, Magnetization transfer contrast (MTC) and tissue water proton relaxation in vivo, Magn. Reson. Med. 10 (1989) 135–144.

[2] K. Ward, A.H. Alertas, R.S. Balaban, A new class of contrast agents for MRI based on proton chemical exchange dependent saturation transfer (CEST), J. Magn. Reson. 143 (2000) 79–87.

[3] K. Ward, R.S. Balaban, Determination of pH using water protons and chemical exchange-dependent saturation transfer (CEST), Magn. Reson. Med. 44 (2000) 799–802.

[4] J. Zhou, J.-F. Payen, D.A. Wilson, R.J. Traystman, P.C.M. van Zijl, Using the amide proton signals of intracellular proteins and peptides to detect pH effects in MRI, Nat. Med. 9 (2003) 1085–1090.

[5] S. Aime, A. Barge, D.D. Castelli, et al., Paramagnetic lanthanide(III) complexes as pH-sensitive chemical exchange saturation transfer (CEST) contrast agents for MRI applications, Magn. Reson. Med. 47 (2002) 639–648.

[6] S. Zhang, L. Michaudet, S. Burgess, A.D. Sherry, The amide protons of an Ytterbium(III) dota tetraamide complex act as efficient antennae for transfer of magnetization to bulk water, Angew. Chem. Int. Ed. 41 (2002) 1919–1921.

[7] S. Aime, D.D. Castelli, E. Terreno, Novel pH-reporter MRI contrast agent, Angew. Chem. Int. Ed. 41 (2002) 4334–4336.

[8] A.P. Dagher, A.H. Alertas, P. Choyke, R.S. Balaban, Imaging of urea using chemical exchange dependent saturation transfer at 1.5T, J. Magn. Reson. Imaging 12 (2000) 745–748.

[9] N. Goffeney, J.W. Bulte, J. Duyn, L.H.J. Bryant, P.C.M. van Zijl, Sensitive NMR detection of cationic-polymer-based gene delivery systems using saturation transfer via proton exchange, J. Am. Chem. Soc. 123 (2001) 8628–8629.

[10] S. Zhang, P. Winter, K. Wu, A.D. Sherry, A novel Europium (III)-based MRI contrast agent, J. Am. Chem. Soc. 123 (2001) 1517–1518.

[11] S. Zhang, K. Wu, A.D. Sherry, Unusually sharp dependence of water exchange rate versus Lanthanide ionic radii for a series of tetraamide complexes, J. Am. Chem. Soc. 124 (2002) 4226–4227.

[12] S. Zhang, M. Merrit, D.E. Woessner, R.E. Lenkinski, A.D. Sherry, PARACEST agents: modulating MRI contrast via water proton exchange, Acc. Chem. Res. 36 (2003) 783–790.

[13] S. Aime, D.D. Castelli, F. Fedeli, E. Terreno, A paramagnetic MRI-CEST agent responsive to lactate concentration, J. Am. Chem. Soc. 124 (2002) 9364–9365.

[14] S. Zhang, R. Trokowski, A.D. Sherry, A paramagnetic CEST agent for imaging glucose by MRI, J. Am. Chem. Soc. 125 (2003) 15288–15289.

[15] H.M. McConnell, Reaction rates by nuclear magnetic resonance, J. Chem. Phys. 35 (1961) 41–48.

[16] D.E. Woessner, S. Zhang, M. Merrit, A.D. Sherry, A numerical solution of the Bloch equations provides insights into the optimal design of PARACEST agents, Magn. Reson. Med. 53 (2005) 790–799.

[17] R.R. Ernst, G. Bodenhausen, A. Wokaun, Dynamic processes studied by two-dimensional exchange spectroscopy, in: J.S. Rowlinson (Ed.), Principles of nuclear magnetic resonance in one and two dimensions, Clarendon Press, Oxford, 1994 (Chapter 9).

[18] S. Mori, C. Abeygunawardana, P.C.M. van Zijl, Water exchange filter with improved sensitivity (WEX II) to study solvent-exchangeable protons: application to the consensus zinc finger peptide CP-1, J. Magn. Reson. B 110 (1996) 96–101.

[19] P.C.M. van Zijl, J. Zhou, N. Mori, J.-F. Payen, S. Mori, Mechanism of magnetization transfer during on-resonance water saturation: a new approach to detect mobile proteins, peptides, and lipids, Magn. Reson. Med. 49 (2003) 440–449.

[20] D. Idiyatullin, S. Michaeli, M. Garwood, Product operator analysis of the influence of chemical exchange on relaxation rates, J. Magn. Reson. 171 (2004) 330–337.

[21] S. Aime, R. Nano, M. Grandi, A new class of contrast agents for magnetic resonance imaging based on selective reduction of water-T2 by chemical exchange, Invest. Radiol. 23 (1988) S267–S270.

[22] B.S. Hu, S.M. Conolly, G.A. Wright, D.G. Nishimura, A. Macovski, Pulsed saturation transfer contrast, Magn. Reson. Med. 26 (1992) 231–240.

[23] E. Schneider, R.W. Prost, G.H. Glover, Pulsed magnetization transfer versus continuous wave irradiation for tissue contrast enhancement, J. Magn. Reson. Imaging 3 (1993) 417–423.

[24] S.J. Graham, R. Henkelman, Understanding pulsed magnetization transfer, J. Magn. Reson. Imaging 7 (1997) 903–912.

[25] M.H. Levitt, Composite pulses, Prog. Nucl. Magn. Reson. Spectrosc. 18 (1986) 61–122.

[26] A.J. Shaka, J. Keeler, T. Frenkiel, R. Freeman, An improved sequence for broadband decoupling: WALTZ-16, J. Magn. Reson. 52 (1983) 335–338.

[27] A.J. Shaka, J. Keeler, R. Freeman, Evaluation of a new broadband decoupling sequence: WALTZ-16, J. Magn. Reson. 53 (1983) 313–340.

[28] O. Trott, D. Abergel, A.G.I. Palmer, An average-magnetization analysis of $R_{1\rho}$ relaxation outside the fast exchange limit, Mol. Phys. 101 (2003) 753–763.

[29] S. Meiboom, Nuclear magnetic resonance study of the proton transfer in water, J. Chem. Phys. 34 (1961) 375–388.

[30] J. Zhou, D.A. Wilson, P.Z. Sun, J.A. Klaus, P.C.M. van Zijl, Quantitative description of proton exchange process between water and endogenous and exogenous agents for WEX, CEST, and APT experiments, Magn. Reson. Med. 51 (2004) 945–952.

[31] A.J. Shaka, J. Keeler, Broadband spin decoupling in isotropic liquids, Prog. Nucl. Magn. Reson. Spectrosc. 19 (1987) 47–64.

[32] D. Abergel, A.G.I. Palmer, On the use of the stochastic Liouville equation in nuclear magnetic resonance: application to $R_{1\rho}$ relaxation in the presence of exchange, Concepts Magn. Reson. A 19 (2003) 134–148.

[33] S. Zhang, A.D. Sherry, Physical characteristics of lanthanide complexes that act as magnetization transfer (MT) contrast agents, J. Solid State Chem. 171 (2003) 38–43.